

Article

An Automatic Motion-Based Artifact Reduction Algorithm for fNIRS in Concurrent Functional Magnetic Resonance Imaging Studies (AMARA-fMRI)

Lia Maria Hocke^{1,2,*} , Yunjie Tong³ and Blaise deBonneval Frederick^{1,2,*}¹ McLean Imaging Center, McLean Hospital, 115 Mill Street, Belmont, MA 02478, USA² Department of Psychiatry, Harvard Medical School, 25 Shattuck St., Boston, MA 02115, USA³ Weldon School of Biomedical Engineering, Purdue University, West Lafayette, IN 47907, USA

* Correspondence: lhocke@mclean.harvard.edu (L.M.H.); bbfrederick@mclean.harvard.edu (B.d.F.)

Abstract: Multimodal functional near-infrared spectroscopy–functional magnetic resonance imaging (fNIRS–fMRI) studies have been highly beneficial for both the fNIRS and fMRI field as, for example, they shed light on the underlying mechanism of each method. However, several noise sources exist in both methods. Motion artifact removal is an important preprocessing step in fNIRS analysis. Several manual motion–artifact removal methods have been developed which require time and are highly dependent on expertise. Only a few automatic methods have been proposed. AMARA (acceleration-based movement artifact reduction algorithm) is one of the most promising automatic methods and was originally tested in an fNIRS sleep study with long acquisition times (~8 h). However, it relies on accelerometry data, which is problematic when performing concurrent fNIRS–fMRI experiments. Most accelerometers are not MR compatible, and in any case, existing datasets do not have this data. Here, we propose a new way to retrospectively determine acceleration data for motion correction methods, such as AMARA in multimodal fNIRS–fMRI studies. We do so by considering the individual slice stack acquisition times of simultaneous multislice (SMS) acquisition and reconstructing high-resolution motion traces from each slice stack time. We validated our method on 10 participants during a memory task (2- and 3-back) with 6 fNIRS channels over the prefrontal cortex (limited field of view with fMRI). We found that this motion correction significantly improved the detection of activation in deoxyhemoglobin and outperformed up-sampled motion traces. However, we found no improvement in oxyhemoglobin. Furthermore, our data show a high overlap with fMRI activation when considering activation in channels according to both deoxyhemoglobin and oxyhemoglobin.

Keywords: fNIRS–fMRI; automatic motion correction; multimodal; AMARA; post-hoc analysis; simultaneous multislice/multiband



check for updates

Citation: Hocke, L.M.; Tong, Y.; Frederick, B.d. An Automatic Motion-Based Artifact Reduction Algorithm for fNIRS in Concurrent Functional Magnetic Resonance Imaging Studies (AMARA–fMRI). *Algorithms* **2023**, *16*, 230. <https://doi.org/10.3390/a16050230>

Academic Editor: Frank Werner

Received: 21 February 2023

Revised: 13 April 2023

Accepted: 25 April 2023

Published: 28 April 2023



Copyright: © 2023 by the authors. Licensee MDPI, Basel, Switzerland. This article is an open access article distributed under the terms and conditions of the Creative Commons Attribution (CC BY) license (<https://creativecommons.org/licenses/by/4.0/>).

1. Introduction

Functional near-infrared spectroscopy (fNIRS) [1] has gained interest in recent years as a noninvasive neuroimaging technique to investigate cortical activity, along with techniques such as functional magnetic resonance imaging (fMRI) and electroencephalography.

fNIRS is thought to indirectly reflect neural activity through neurovascular coupling by detecting changes in light scattering and absorption within the tissue caused by changes in the concentration of oxyhemoglobin (ΔHbO) and deoxyhemoglobin (ΔHb). Besides fNIRS' many practical advantages such as portability, compatibility with other techniques, no requirements for a special environment, and no restriction on the subject population, its technical advantages lie in its temporal resolution (~25 to 100 Hz) of hemoglobin concentration measurements (practically only restricted by the hemodynamic response function itself) and the ability to distinguish between both chromophores, oxyhemoglobin, and deoxyhemoglobin. However, major challenges include (1) relatively poor spatial resolution (1 to 3 cm³) caused by the scattering of light in tissue and the geometry of

the light sources and detectors on the surface of the head which can only be alleviated with a dense cluster of overlapping channels; (2) the limited penetration depth (1 cm of cerebral cortex [2]); and (3) contamination from noise sources including instrumental noise, experimental noise, and physiological artifacts [3]. Hence, one of the greatest challenges in fNIRS research is the accurate delineation of the masking effects of the noise sources from the desired “neuronal” brain signal.

Functional magnetic resonance imaging (fMRI) has long been the gold standard of non-invasive brain imaging due to its high spatial resolution over the whole head. Since the development of multiband/simultaneous multislice (SMS) acquisition [4,5], simultaneous high spatial (1–2 mm isotropic) and temporal resolution (~0.7 s) are now possible. fMRI exploits the effect of blood oxygenation on the magnetic properties of hemoglobin, just as fNIRS uses the effect on its optical properties, to make inferences about underlying neuronal activity changes in the brain; however, it lacks the ability to separately quantify oxyhemoglobin and deoxyhemoglobin changes and still struggles to approach the temporal resolution of fNIRS (resulting in the poor quantification of cardiac effects). Due to the complementary strengths of fNIRS and fMRI in temporal and spatial resolution, respectively, multimodal studies often utilize fNIRS and fMRI simultaneously which has shed light on various aspects of each method [6].

Since fNIRS optodes are directly positioned on the scalp of the participant, fNIRS is in general considered less sensitive to head motion artifacts than fMRI, which depend on stationary sensors. However, motion artifacts are still a problem for fNIRS because the coupling between the optodes and the skin is altered when the optode is displaced. This introduces a strong external noise which produces spurious differences that can mask patterns arising from neural activity. Therefore, despite the relative insensitivity of fNIRS to head motion, it is still necessary to apply processing strategies that eliminate these artifacts. A wide variety of motion artifact elimination techniques have been proposed ([7,8]). These techniques can be categorized based on the temporal or spatial characteristics of the signal and methods that use external signals for movement artifact removal by adaptive filtering.

The motion-correction algorithms, which have been developed for fNIRS data, suffer from different drawbacks. For example, some of the wavelet-based methods (e.g., [9,10]) are well equipped to remove motion spikes; however, exacerbate baseline shifts artifacts. Especially, methods relying on global temporal characteristics (such as PCA-based methods) require a certain number of channels to perform accurate delineation between the noise and signal, as do spatially based methods. Other methods such as the Movement Artifact Reduction Algorithm (MARA) [11] rely on several parameters that must be supplied by the user to detect artifacts, which is usually disadvantageous. AMARA (acceleration-based movement artifact reduction algorithm) [12] is one of those methods but also one of the most promising automatic motion correction methods for fNIRS analysis. The method identifies motion artifacts using an accelerometer and combines two previous motion detection and removal methods, MARA [11] and ABAMAR [13]. It has been tested on long fNIRS sleep study acquisitions (~8 h) and compares favorably to both MARA and ABAMAR.

Motion displacement parameters can be easily acquired from fMRI with FSL MCFLIRT [14,15] or AFNI 3dvolReg [16,17], two standard pre-processing programs for fMRI data. The second derivative of the motion time courses of fMRI can therefore be used to determine the acceleration-based movement in fNIRS. However, here, the relatively low temporal resolution of fMRI is problematic; it would be highly advantageous if the acceleration time courses could be derived at the same, much higher temporal resolution of the fNIRS data.

Here, we propose a new way to increase the temporal resolution of acceleration data derived from the fMRI motion measurements. We do so by adapting and expanding a method we developed for increasing the time resolution of motion data in fMRI by taking into account the slice acquisition time and reconstructing high-resolution motion time courses [18]. Similar techniques have been proposed using slice-wise motion correction [19] and have been applied for real-time motion correction [20,21] with slice-to-volume registra-

tion in which guided breath-hold at 0.34 Hz could be observed in one subject [20]. These techniques, such as the one by Hoinkiss et al. [20], rely on advanced iterative algorithms. Our technique was developed to reconstruct respiration, as a complement to our cardiac waveform reconstruction method [22] using slice sorted averaging and a deep learning reconstruction filter. Although a deep learning approach was highly successful in our previous work and our current method might benefit from that, in this situation, unlike the cardiac waveform generation, we did not have ground truth high-frequency motion data. However, this method performs very well, reconstructing respiration, cardiac, and high-resolution motion without requiring any advanced modeling and instead by simply reorganizing slices according to their acquisition times [18]. Machine learning is especially useful for extrapolating information which is not directly available in a particular dataset by automatically finding patterns and interrelationships within datasets in the absence of a model, and then applying this to fill in missing information. However, when there are known characteristics of the system (in this case, that the head is a rigid structure and motion of one part of the head means that the rest of the head undergoes similar motion), it is always preferable to incorporate this information to minimize the degree to which the other parts of the system need to “learn” these relationships.

Here, we incorporate this information into deriving a better motion time course, so that AMARA is more firmly within the regime that it was developed to handle (that certain types of motion cause transients in fNIRS data that can be removed). In the following, we show how this method can be used in conjunction with automatic motion correction methods in fNIRS such as AMARA in order to enhance signal detection.

2. Materials and Methods

We measured fNIRS and fMRI simultaneously in 10 participants during a 2- and 3-back memory task (720 s, Figure 1e). All subjects gave their informed consent for inclusion before they participated in the study. The McLean Hospital institutional review board approved all human experimental acquisitions, and participants were compensated for their participation.

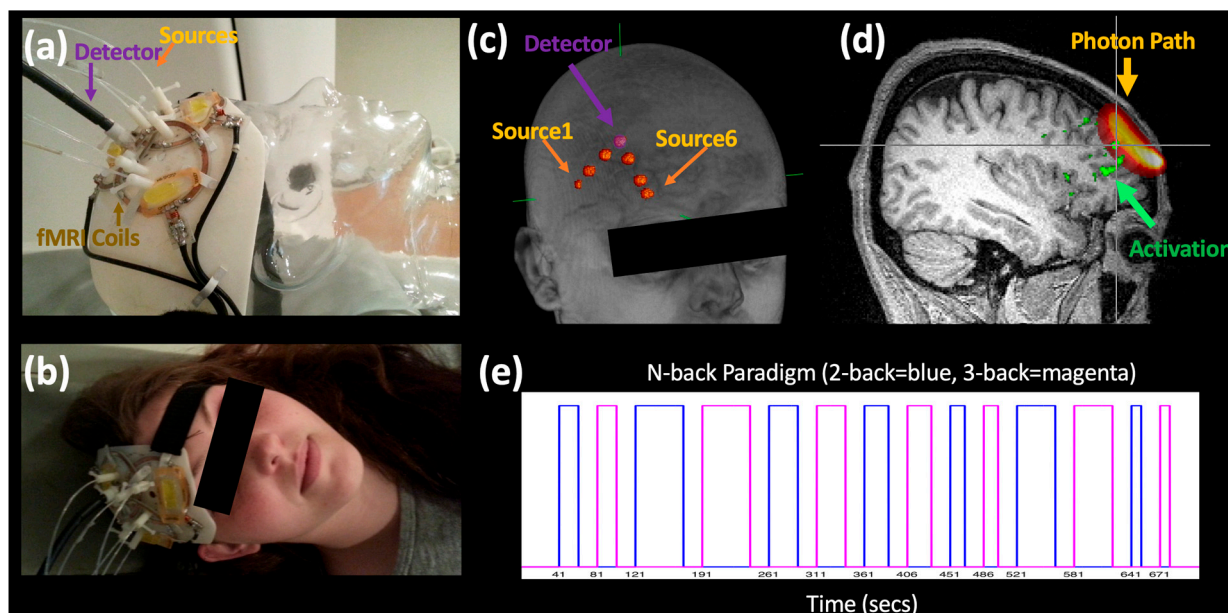


Figure 1. Set-Up. (a,b) Multimodal fNIRS–fMRI coil with six sources and one detector positioned over the prefrontal cortex. (c) Sources and the detector could be easily localized on anatomical scans and (d) the photon path of each channel was calculated. (e) The stimulation paradigm for the N-back task (shown here) is shown.

Six fNIRS source–detector fibers were directly integrated into purpose-built 3D printed receive-only phased array RF coils [23], enabling close contact between the probe and the head and thus the precise alignment between the modalities, facilitating localization of the fNIRS probes with respect to the activations detected by fMRI (Figure 1a–c).

All MR data were acquired on a Siemens TIM Trio 3T scanner (Siemens Medical Systems, Malvern, PA, USA). The multimodal probe included a 3-element receive-only phased array probe (8×4.5 cm with depth sensitivity of ~ 5 cm) [23] which was positioned over the prefrontal cortex and used to acquire high spatial (1.8 mm isotropic resolution over a $172 \times 172 \times 59.4$ mm FOV) and temporal resolution fMRI data ($TR = 0.72$ s, Multiband Factor = 4). fNIRS data were acquired with an ISS Imagent (ISS, Champaign, IL, USA) at 6.25 Hz with six channels (~ 35 , 27, and 13 mm source–detector separation, Table 1) above the target area.

Table 1. Source–Detector Separation (in mm).

Subject	Channel 1	Channel 2	Channel 3	Channel 4	Channel 5	Channel 6
#1	37.3	28.2	13.0	13.0	28.0	39.0
#2	35.9	27.3	11.8	15.5	28.6	40.2
#3	37.0	28.6	13.6	17.0	29.2	37.0
#4	35.9	26.2	10.4	14.3	24.4	34.7
#5	37.8	27.0	12.2	14.6	29.1	37.8
#6	35.4	25.1	12.1	13.7	29.0	37.0
#7	34.1	25.5	11.4	13.1	28.6	42.2
#8	35.4	28.5	12.6	13.2	29.6	37.3
#9	35.6	25.6	11.9	18.0	26.9	36.6
#10	38.0	24.6	12.9	16.4	30.2	39.6

High-resolution motion traces were calculated using our previously described method (for a detailed description of the steps and commands see Hocke et al. [18]). In short, since multiband data have several spatially separated slices acquired at the same time, the exact acquisition time or slice timing information of each slice (indicated by different colors in Figure 2a) can be used to split a single fMRI volume into “stacks” of simultaneously acquired slices. In the simplified example of Figure 2, 20 slices are taken at 5 different acquisition times with a multiband factor of 4, resulting in 5 stacks with the same acquisition time, as illustrated in different colors in Figure 2a. Standard motion estimation programs for fMRI data (e.g., FSL [24], MCFLIRT) are then applied to each new stack of acquisition–time matched slices (Figure 2b). Lastly, the various motion traces (six directions for each stack) can then be merged according to their respective slice timing (Figure 2c). A comparison with simultaneously acquired physiological monitoring confirmed the accuracy of this method, recovering even signals beyond the original frequency range such as cardiac (Figure 2d). A software package deriving these high-resolution motion parameters, as described above and in Hocke et al. [18], can be found as open source by P. Bloom [25]. A notch filter at the original sampling rate was also applied.

Acceleration data were derived from the second derivative of the motion traces of the high-resolution fMRI data. We used MCFLIRT (FSL [24], FLIRT [14,15]), a standard fMRI preprocessing method to derive the six motion traces (x, y, z direction as well as rotational motion of each). We used the six acceleration motion traces as inputs for AMARA with window length of 8 min and window step size of 4 min (for our 12 min acquisition) which were in the originally published study by Metz et al. set to 15 min and 5 min, respectively [12].

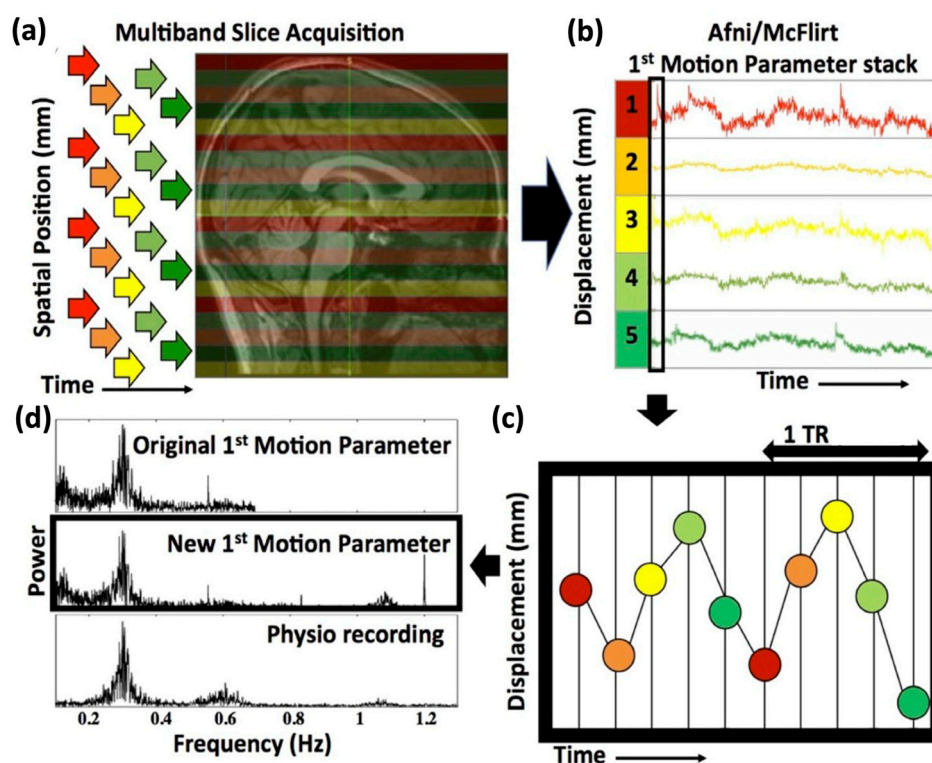


Figure 2. Calculation of the high-resolution motion traces. (a) Multiple slices (arrows in the same color) are taken at different time points (arrows in different colors) according to the multiband factor. (b) When calculating the motion parameters for each slice time ‘stack’ (the set of simultaneously obtained images at a timepoint, e.g., those specified by the red arrows), the sampling rate can be increased by the number of independent slice times and (c) their reorganization according to their acquisition time (d) so that physiological signals (e.g., cardiac) can be resolved at higher frequencies (software available by P. Bloom [25]). Figure replicated and slightly modified from Hocke et al. [18].

Raw fNIRS data were converted to oxyhemoglobin and deoxyhemoglobin with HOMER2 [3]. The pathlength was corrected in accordance with the source–detector distance calculated from the fMRI anatomical scans and also corrected for age [26]. We compared three motion correction conditions: no motion correction (NoMC); simple up-sampled motion correction (UpMC) in which the OrigRes motion time courses were up-sampled to the effective sampling rate by using the `scipy.interpolate’s UnivariateSpline` routine with the default smoothing ($k = 3$); and correction with high-resolution motion traces (HighMC with AMARA–fMRI). The significance of the activation of each channel per method was calculated with the NIRS Brain AnalyzIR Toolbox [27] which accounts for multiple comparisons (q-stats). Significant task responses determined by fMRI (example voxels in Figure 3a) were evaluated below the fNIRS channel in the photon paths calculated using MCX [28,29]. We calculated the percentage of significant voxels present in the photon path (banana-shaped) activation area below the fNIRS probes (Figure 4c) as well as the z-statistics (Figure 4b) for comparison.

MRI data were processed in FSL FEAT [FMRIB Expert Analysis Tool, version 5.0.10 (<http://www.fmrib.ox.ac.uk/fsl>, accessed on 20 February 2023, Oxford University, United Kingdom [24]). Standard preprocessing steps were applied to the data: temporal high-pass filter (200 s to remove very slow instrumental drifts), spatial smoothing (2 mm), slice time correction, motion correction, and FILM prewhitening. Contrasts for both the 2- and 3-back as well as only the 2-back and 3-back were evaluated for comparison (1st contrast: 2-back = 1, 3-back = 1; 2nd contrast: 2-back = 1, 3-back = 0; and 3rd contrast: 2-back = 0, 3-back = 1).

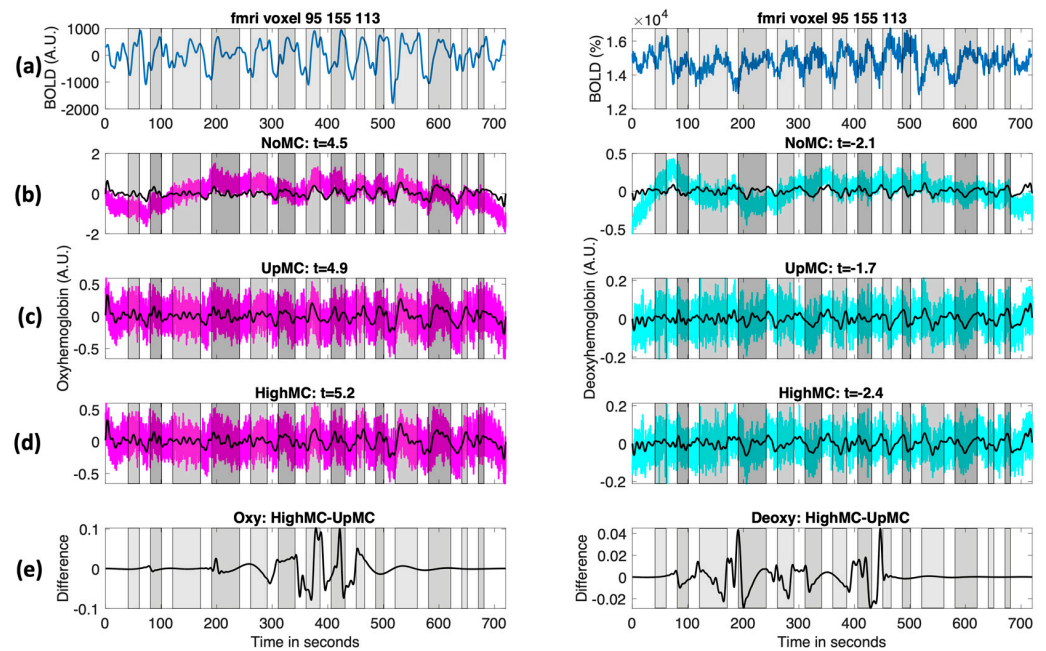


Figure 3. Example time courses. Example time course from subject #4 showing (a) an underlying fMRI voxel activation pattern within the photon probability path (MCX) and (b–d) the fNIRS time course filtered at $\sim 0.0015\text{--}2$ Hz (background magenta (oxyhemoglobin), cyan (deoxyhemoglobin)), and $\sim 0.015\text{--}0.1$ Hz (black signal). Specifically, (b) the original fNIRS time course is shown without motion correction (NoMC) as well as (c) the motion corrected with AMARA using the up-sampled (UpMC) and (d) reconstructed high sample rate motion time courses (HighMC) from fMRI. T-statistics are shown in the title (“t”). (e) Lastly, the difference between the HighMC and UpMC fNIRS time courses at $\sim 0.015\text{--}0.1$ Hz is shown.

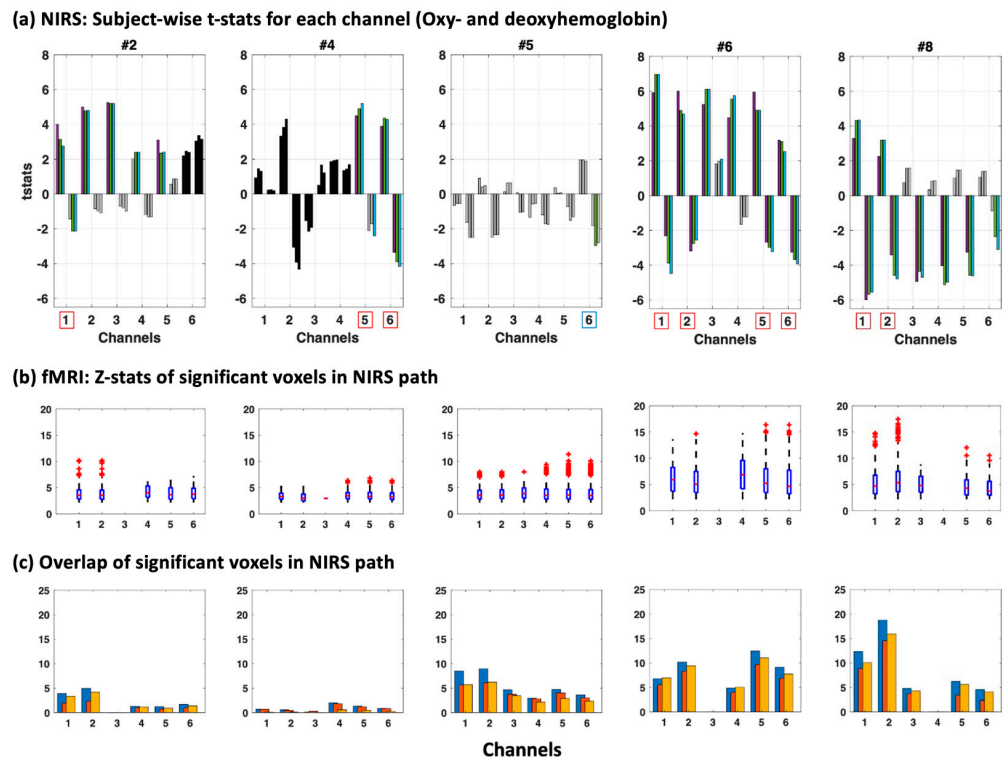


Figure 4. Significant fNIRS activation and comparison of fMRI data. T-statistics (a) with significant activation for all three motion correction methods (lilac, NoMC; green, UpMC; and blue, HighMC)

and without reaching significance (grey) or being excluded for data quality purposes (black). In addition, (b) z-statistics distribution underneath channels one through to six within the photon probability path (MCX) as well as (c) the percentage overlap of the photon path and significantly activated voxels in fMRI (with 3 different contrasts) for each subject.

3. Results

We calculated high temporal resolution motion parameters by dividing the original multiband fMRI brain images, taken with TR of 0.72 s, into the 9 sets, or ‘stacks’, of simultaneously acquired images acquired within each TR at 9 “slice times” (72 slices with a multiband factor of 8 corresponds to 9 sets of slices acquired at 9 different slice or acquisition times), and merging the resulting time course of the 9 stacks for each motion parameter (total 6) according to the slice timing (Figure 2) [18]. This resulted in an effective sample rate of 12.5 Hz. Notably, even by using initial motion traces with a sample time of 0.72 s (1.4 Hz sampling rate, with a Nyquist frequency of 0.7 Hz), for which the cardiac signal at ~1 Hz could not be resolved, we could now resolve the cardiac signal (Figure 2). Figure 3 shows an example of the resulting fNIRS time course with and without motion correction (Figure 3b–d) as well as an example an fMRI time course in the sensitive region of the fNIRS probe (Figure 3a).

We also compared our fNIRS results to the fMRI data (Figure 4 and for all subjects see Figure A1) including the z-statistics in the photon probability path underneath the channels (Figure 4b) as well as the overlap between the photon probability path and the significantly activated voxels seen in fMRI (Figure 4c) for three contrasts of the N-back task (1st contrast: 2-back = 1, 3-back = 1; 2nd contrast: 2-back = 1, 3-back = 0; 3rd contrast: 2-back = 0, 3-back = 1).

We found a high consensus in most subjects with high z-statistics ($z > 10$) in areas with even a small percentage overlap with fMRI (~above 5%) when taking both oxyhemoglobin and deoxyhemoglobin into account (red boxes around channels below the x-axis in Figure 4a), except in subject #4 and #5. Subject 5 was especially affected by motion which may explain the improved t-statistics with motion correction (for deoxyhemoglobin). However, even though t-statistics were high for both oxyhemoglobin and deoxyhemoglobin for Subject 5 channel 6, the significance threshold was not reached when multiple comparison correction was applied (blue box around channel in which significance was reached without multiple comparison correction).

Changes in the t-statistics of the task response with motion correction (with up-sampled (UpMC) and reconstructed high sample rate (HighMC) motion parameters) in comparison to without motion correction (NoMC) were compared in all 10 subjects both for oxyhemoglobin and deoxyhemoglobin. For this evaluation, we considered the 18 non-significant channels (no significant changes in oxyhemoglobin or deoxyhemoglobin changes with any method, Figure 5a,b) and the 9 significant channels (both significant oxyhemoglobin and deoxyhemoglobin changes, Figure 5c,d) separately and disregarded channels in which only oxyhemoglobin or deoxyhemoglobin showed significant activation with any method.

Non-significant channels ($N = 18$) for oxyhemoglobin in the NoMc and UpMC condition did not differ significantly from HighMC (one-sided *t*-test, $p < 0.09$ and $p < 0.48$, respectively) (Figure 5a) and neither did non-significant channels for deoxyhemoglobin (one-sided *t*-test, $p < 0.56$ and $p < 0.11$, respectively) (Figure 5b). Mean \pm Std t-statistics for non-significant oxyhemoglobin channels in all three motion correction methods were 0.54 ± 1.0 (NoMC), 0.81 ± 1.0 (UpMC), and 0.81 ± 1.0 (HighMC) (Figure 5a) and for non-significant deoxyhemoglobin channels -0.17 ± 1.1 (NoMC), -0.11 ± 1.4 (UpMC), and -0.15 ± 1.4 (HighMC) (Figure 5b).

Significant channels ($N = 9$) for oxyhemoglobin in the NoMc and UpMC condition did not differ significantly from HighMC (one-sided *t*-test, $p < 0.51$ and $p < 0.87$, respectively) (Figure 5c); however, significant channels for deoxyhemoglobin did (one-sided *t*-test, $p < 0.03$ and $p < 0.03$, respectively) (Figure 5d). Mean \pm Std t-statistics for significant

oxyhemoglobin channels in all three motion correction methods were 4.33 ± 1.4 (NoMC), 4.42 ± 1.2 (UpMC), and 4.3 ± 1.4 (HighMC) (Figure 5c) and for significant deoxyhemoglobin channels were -3.08 ± 1.3 (NoMC), -3.48 ± 1.2 (UpMC), and -3.70 ± 1.2 (HighMC) (Figure 5d).

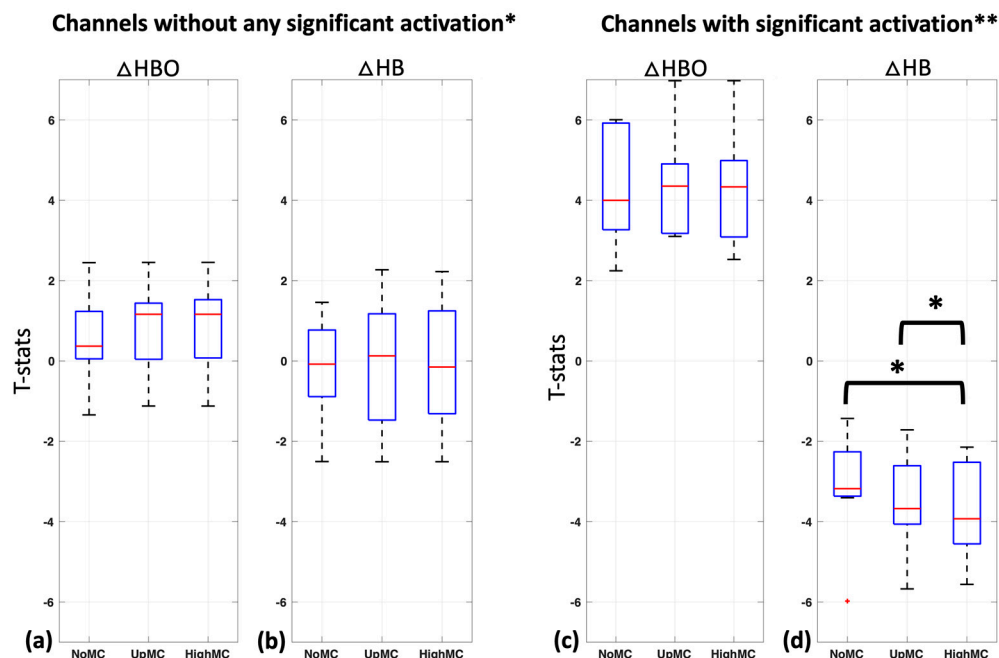


Figure 5. Comparison of motion correction methods. (a,b) T-statistics of channels without motion correction (NoMC) and with up-sampled (UpMC) and reconstructed high sample rate motion correction (HighMC) in all non-significant channels (* no significant changes in oxyhemoglobin or deoxyhemoglobin changes with any method, $N = 18$) and (c,d) significant channels (** significant channels were only considered significant when both oxyhemoglobin and deoxyhemoglobin were significant in any method, $N = 9$), over 10 participants. We only found a significant difference (one-sided t -test with an alpha of 0.05) in the t -statistics for deoxygenated hemoglobin between NoMC and UpMC in comparison to HighMC ($p < 0.03$ and $p < 0.03$) in the significant channels.

4. Discussion

In this study, we demonstrate a new way to use high-resolution motion time courses extracted from fMRI to generate acceleration input data for the fNIRS motion correction methods, such as AMARA (acceleration-based movement artifact reduction algorithm) [12] in multimodal fNIRS–fMRI studies. We did so by increasing the effective temporal resolution of acceleration data derived from the fMRI motion measurements, by adapting and expanding a method we developed to extract motion parameters at the slice acquisition time resolution, rather than the volume acquisition time resolution [18]. We call this method AMARA–fMRI. We tested this method on a small number of channels, with a window length and step size representative of concurrent fNIRS/fMRI research datasets (~10 min), rather than the parameters used in the original sleep study on long acquisition times with a window length of 15 min [12].

We found that this high-resolution motion correction method (HighMC) significantly improved the detection of activation in deoxyhemoglobin in comparison to no motion correction (NoMC) in the channels with significant activation (significant channels were only considered significant when both oxyhemoglobin and deoxyhemoglobin were significant for any method—red boxes in Figure 4a) shown in Figure 5d; the method also outperformed simple up-sampled motion traces converted into acceleration data (UpMC) in these channels (Figure 5d). As expected, this was not true for channels showing no activation pattern (defined as channels with neither oxyhemoglobin nor deoxyhemoglobin

showing significant activation with any method). This fact, in conjunction with the fact that we do not see “significant activation patterns” in any of the very small source–detector distances (e.g., channels 3 and 4) which are considered to probe only more superficial layers of the brain (e.g., [30,31]), is encouraging. This suggests that this motion correction does not simply increase the t-statistics in all the channels it is applied to or introduce patterns resembling activation; rather, it specifically unmasks patterns of underlying neuronal activity, increasing only the t-statistics for these channels.

Notably, in most channels AMARA–fMRI performed very well on deoxyhemoglobin measures, even rendering channels significant, which would not have been significant without correction (see Figure 4a, Subject #2, channel 1). Studies have demonstrated that changes in the deoxyhemoglobin concentration detected in fNIRS provide a more accurate reflection of underlying neuronal activation, particularly in the spatial domain. This is in comparison to the calculation of activation maps using oxyhemoglobin. As a result, improving the signal quality of deoxyhemoglobin can greatly enhance the accuracy of fNIRS results [32–34].

Furthermore, the fNIRS results were mostly in accordance with the underlying pattern of neuronal activity revealed by the fMRI data (Figure 4 and for all subjects Figure 1A), in accordance with previously reported overlaps between both techniques [6,23,35–38]. It also showed that even spatially small activation patterns, in combination with high z-statistics in fMRI, predicted fNIRS activation patterns in the channels above the activation site. However, we did see that in Subject #5 the motion effects could not be completely resolved with AMARA–fMRI to reveal the underlying neuronal activation shown with fMRI. This subject had a very high amount of motion in all channels, and although motion correction increased t-statistics in deoxyhemoglobin, it did not meet the significance threshold when corrected for multiple comparisons. This does suggest limitations on the amount of motion that can be removed; however, these limitations are relevant only with very strong motion artifacts.

Besides these limitations, there are also additional limiting factors to our method. Namely, since our method relies on extracting the maximum amount of motion information possible from the fMRI data by measuring motion in sub-timepoints of the TR, our method will fail in cases where (1) the fMRI acquisition method does not allow for three-dimensional sub-TR motion estimation, for example if a non-multiband acquisition is used; (2) the multiband factor is too low to get good motion estimates from the subsampled data (the slice stacks are too coarse to estimate motion reliably); or (3) the multiband factor is too high, so the degree of subsampling within a TR is too low to give an effective boost to the sample rate.

Lastly, these results are based on a very small number of channels, making this method well adapted to multimodal experiments in which only a small number of channels are used due to the set-up time, subject comfort, and head position when lying down among other reasons. Motion correction methods based on global temporal filtering may perform poorly in these instances. Though these are very promising results, we did not observe a significant improvement in the oxyhemoglobin activations. This is most likely due to the higher initial signal-to-noise ratio of oxyhemoglobin; in voxels with significant activation, the signal was most likely already detected, so improved motion correction would not be expected to make a large difference (Figure 3e). There may also be an influence attributable to the window length and step size chosen. AMARA was originally designed for extremely long free-moving studies, with window length and step size of 15 min and 5 min, respectively. The multimodal fMRI studies are restricted in terms of their motion and are of much shorter duration (e.g., commonly used paradigm times of approximately 10 min), so we would expect them to require significantly different tuning parameters than the original reference. We arrived at the chosen values using an exhaustive hyperparameter search on a single subject in a preliminary study [39]. Incidentally, we saw here that a higher window length of 10, with step size of 5 min, was more advantageous for oxyhemoglobin. While the values we selected are clearly effective at improving the power of task detection

in an existing dataset, repeating the procedure in a larger, more heterogeneous dataset encompassing more subjects and a variety of tasks will be required to tune these values optimally. However, this was beyond the scope and power of the current study.

Author Contributions: Conceptualization, L.M.H.; methodology, L.M.H.; software, L.M.H.; validation; formal analysis, L.M.H.; investigation, L.M.H.; resources, L.M.H. and B.d.F.; data curation, L.M.H., Y.T. and B.d.F.; writing—original draft preparation, L.M.H.; writing—review and editing, L.M.H., B.d.F. and Y.T.; visualization, L.M.H.; supervision, L.M.H. and B.d.F.; project administration, L.M.H. and B.d.F.; funding acquisition, L.M.H. and B.d.F. All authors have read and agreed to the published version of the manuscript.

Funding: This research was funded by NIH/NIA under grant number R21 AG070383-01 (LMH) and NIH/NIHM under grant number RF1 MH130637-01 (BBF).

Data Availability Statement: The data and results of this paper are not shared since consent was not given for sharing data and was not requested in the original IRB. The code to transform the motion parameters of multislice imaging into high-resolution motion time courses is available as open software by P. Bloom [25].

Conflicts of Interest: The authors declare no conflict of interest.

Appendix A

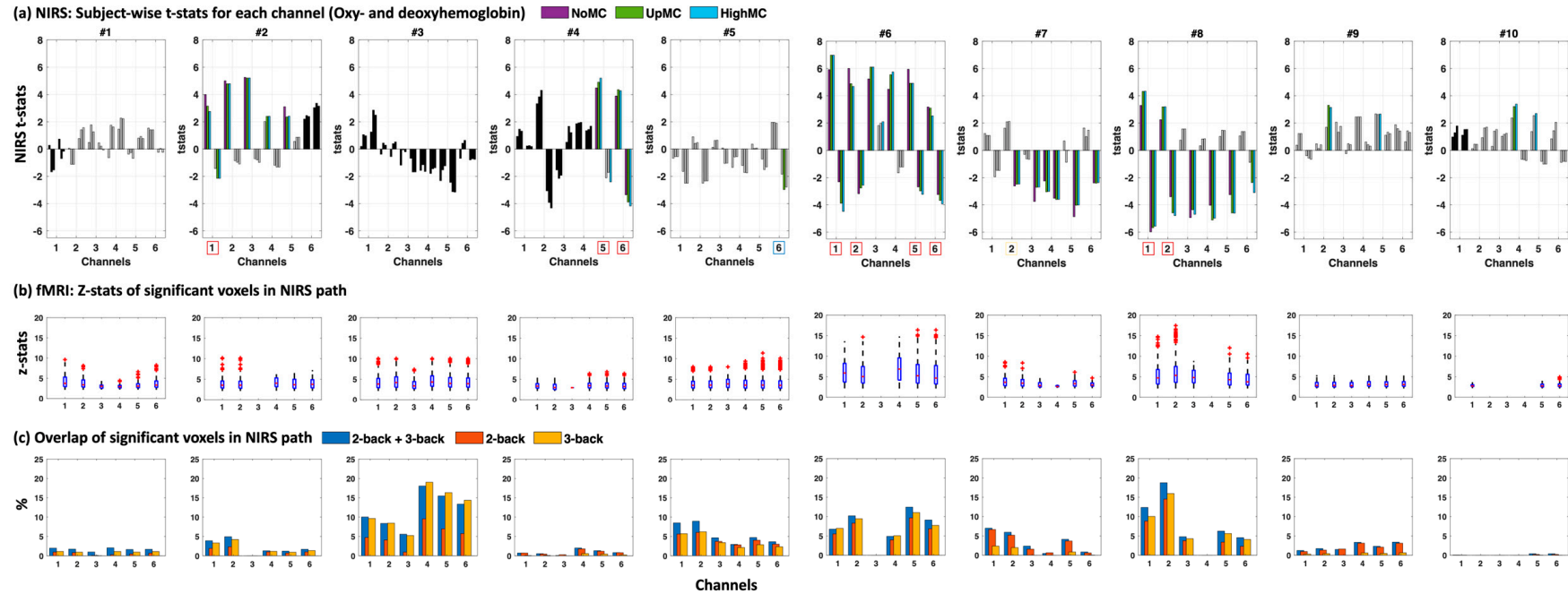


Figure A1. Figure 4 extension—overview and comparison of fMRI data. T-statistics (a) with significant activation for all three motion correction methods (lilac, NoMC; green, UpMC; and blue, HighMC) and without reaching significance (grey) or being excluded for data quality purposes (black). In addition (b) z-statistics distribution underneath channels one through to six within the photon probability path (MCX) as well as (c) percentage overlap of photon path and significantly activated voxels in fMRI (with three different contrasts) for each subject.

References

1. Jobsis, F.F. Noninvasive, infrared monitoring of cerebral and myocardial oxygen sufficiency and circulatory parameters. *Science* **1977**, *198*, 1264. [[CrossRef](#)] [[PubMed](#)]
2. Boas, D.A.; Chen, K.; Grebert, D.; Franceschini, M.A. Improving the diffuse optical imaging spatial resolution of the cerebral hemodynamic response to brain activation in humans. *Opt. Lett.* **2004**, *29*, 1506–1508. [[CrossRef](#)] [[PubMed](#)]
3. Huppert, T.J.; Diamond, S.G.; Franceschini, M.A.; Boas, D.A. HomER: A review of time-series analysis methods for near-infrared spectroscopy of the brain. *Appl. Opt.* **2009**, *48*, D280–D298. [[CrossRef](#)]
4. Feinberg, D.A.; Moeller, S.; Smith, S.M.; Auerbach, E.; Ramanna, S.; Gunther, M.; Glasser, M.F.; Miller, K.L.; Ugurbil, K.; Yacoub, E. Multiplexed echo planar imaging for sub-second whole brain fMRI and fast diffusion imaging. *PLoS ONE* **2010**, *5*, e15710. [[CrossRef](#)]
5. Moeller, S.; Yacoub, E.; Olman, C.A.; Auerbach, E.; Strupp, J.; Harel, N.; Ugurbil, K. Multiband multislice GE-EPI at 7 tesla, with 16-fold acceleration using partial parallel imaging with application to high spatial and temporal whole-brain fMRI. *Magn. Reson. Med.* **2010**, *63*, 1144–1153. [[CrossRef](#)]
6. Steinbrink, J.; Villringer, A.; Kempf, F.; Haux, D.; Boden, S.; Obrig, H. Illuminating the BOLD signal: Combined fMRI-fNIRS studies. *Magn. Reson. Imaging* **2006**, *24*, 495–505. [[CrossRef](#)] [[PubMed](#)]
7. Brigadoi, S.; Ceccherini, L.; Cutini, S.; Scarpa, F.; Scatturin, P.; Selb, J.; Gagnon, L.; Boas, D.A.; Cooper, R.J. Motion artifacts in functional near-infrared spectroscopy: A comparison of motion correction techniques applied to real cognitive data. *Neuroimage* **2014**, *85 Pt 1*, 181–191. [[CrossRef](#)]
8. Cooper, R.J.; Selb, J.; Gagnon, L.; Phillip, D.; Schytz, H.W.; Iversen, H.K.; Ashina, M.; Boas, D.A. A systematic comparison of motion artifact correction techniques for functional near-infrared spectroscopy. *Front. Neurosci.* **2012**, *6*, 147. [[CrossRef](#)]
9. Chiarelli, A.M.; Maclin, E.L.; Fabiani, M.; Gratton, G. A kurtosis-based wavelet algorithm for motion artifact correction of fNIRS data. *Neuroimage* **2015**, *112*, 128–137. [[CrossRef](#)]
10. Molavi, B.; Dumont, G.A. Wavelet-based motion artifact removal for functional near-infrared spectroscopy. *Physiol. Meas.* **2012**, *33*, 259–270. [[CrossRef](#)]
11. Scholkmann, F.; Spichtig, S.; Muehlemann, T.; Wolf, M. How to detect and reduce movement artifacts in near-infrared imaging using moving standard deviation and spline interpolation. *Physiol. Meas.* **2010**, *31*, 649–662. [[CrossRef](#)] [[PubMed](#)]
12. Metz, A.J.; Wolf, M.; Achermann, P.; Scholkmann, F. A New Approach for Automatic Removal of Movement Artifacts in Near-Infrared Spectroscopy Time Series by Means of Acceleration Data. *Algorithms* **2015**, *8*, 1052–1075. [[CrossRef](#)]
13. Virtanen, J.; Noponen, T.; Kotilahti, K.; Virtanen, J.; Ilmoniemi, R.J. Accelerometer-based method for correcting signal baseline changes caused by motion artifacts in medical near-infrared spectroscopy. *J. Biomed. Opt.* **2011**, *16*, 087005. [[CrossRef](#)] [[PubMed](#)]
14. Jenkinson, M.; Smith, S. A global optimisation method for robust affine registration of brain images. *Med. Image Anal.* **2001**, *5*, 143–156. [[CrossRef](#)]
15. Jenkinson, M.; Bannister, P.; Brady, M.; Smith, S. Improved optimization for the robust and accurate linear registration and motion correction of brain images. *Neuroimage* **2002**, *17*, 825–841. [[CrossRef](#)]
16. Cox, R.W. AFNI: Software for analysis and visualization of functional magnetic resonance neuroimages. *Comput. Biomed. Res.* **1996**, *29*, 162–173. [[CrossRef](#)]
17. Cox, R.W.; Jesmanowicz, A. Real-time 3D image registration for functional MRI. *Magn. Reson. Med.* **1999**, *42*, 1014–1018. [[CrossRef](#)]
18. Hocke, L.M.; Frederick, B.B. Post-hoc physiological waveform extraction from motion estimation in simultaneous multislice (SMS) functional MRI using separate stack processing. *Magn. Reson. Med.* **2021**, *85*, 309–315. [[CrossRef](#)]
19. Beall, E.B.; Lowe, M.J. SimPACE: Generating simulated motion corrupted BOLD data with synthetic-navigated acquisition for the development and evaluation of SLOMOCO: A new, highly effective slice-wise motion correction. *Neuroimage* **2014**, *101*, 21–34. [[CrossRef](#)]
20. Hoinkiss, D.C.; Erhard, P.; Breutigam, N.J.; von Samson-Himmelstjerna, F.; Gunther, M.; Porter, D.A. Prospective motion correction in functional MRI using simultaneous multislice imaging and multislice-to-volume image registration. *Neuroimage* **2019**, *200*, 159–173. [[CrossRef](#)]
21. Teruel, J.R.; Kuperman, J.M.; Dale, A.M.; White, N.S. High temporal resolution motion estimation using a self-navigated simultaneous multi-slice echo planar imaging acquisition. *J. Magn. Reson. Imaging* **2018**, *48*, 780–787. [[CrossRef](#)] [[PubMed](#)]
22. Aslan, S.; Hocke, L.M.; Schwarz, N.; Frederick, B. Extraction of the cardiac waveform from simultaneous multislice fMRI data using slice sorted averaging and a deep learning reconstruction filter. *Neuroimage* **2019**, *198*, 303–316. [[CrossRef](#)] [[PubMed](#)]
23. Hocke, L.M.; Cayetano, K.; Tong, Y.; Frederick, B. Optimized multimodal functional magnetic resonance imaging/near-infrared spectroscopy probe for ultrahigh-resolution mapping. *Neurophotonics* **2015**, *2*, 045004. [[CrossRef](#)] [[PubMed](#)]
24. Smith, S.M.; Jenkinson, M.; Woolrich, M.W.; Beckmann, C.F.; Behrens, T.E.; Johansen-Berg, H.; Bannister, P.R.; De Luca, M.; Drobnjak, I.; Flitney, D.E.; et al. Advances in functional and structural MR image analysis and implementation as FSL. *Neuroimage* **2004**, *23* (Suppl. S1), S208–S219. [[CrossRef](#)] [[PubMed](#)]
25. Bloom, P.A. Available online: https://github.com/pab2163/estimate_respiratory_traces.git (accessed on 20 February 2023).
26. Scholkmann, F.; Wolf, M. General equation for the differential pathlength factor of the frontal human head depending on wavelength and age. *J. Biomed. Opt.* **2013**, *18*, 105004. [[CrossRef](#)] [[PubMed](#)]
27. Santosa, H.; Zhai, X.; Fishburn, F.; Huppert, T. The NIRS Brain AnalyzIR Toolbox. *Algorithms* **2018**, *11*, 73. [[CrossRef](#)]

28. Fang, Q.; Boas, D.A. Monte Carlo simulation of photon migration in 3D turbid media accelerated by graphics processing units. *Opt. Express* **2009**, *17*, 20178–20190. [[CrossRef](#)]
29. Yu, L.; Nina-Paravecino, F.; Kaeli, D.; Fang, Q. Scalable and massively parallel Monte Carlo photon transport simulations for heterogeneous computing platforms. *J. Biomed. Opt.* **2018**, *23*, 010504. [[CrossRef](#)]
30. Wyser, D.; Mattille, M.; Wolf, M.; Lamercy, O.; Scholkmann, F.; Gassert, R. Short-channel regression in functional near-infrared spectroscopy is more effective when considering heterogeneous scalp hemodynamics. *Neurophotonics* **2020**, *7*, 035011. [[CrossRef](#)]
31. Santosa, H.; Zhai, X.; Fishburn, F.; Sparto, P.J.; Huppert, T.J. Quantitative comparison of correction techniques for removing systemic physiological signal in functional near-infrared spectroscopy studies. *Neurophotonics* **2020**, *7*, 035009. [[CrossRef](#)]
32. Defenderfer, J.; Kerr-German, A.; Hedrick, M.; Buss, A.T. Investigating the role of temporal lobe activation in speech perception accuracy with normal hearing adults: An event-related fNIRS study. *Neuropsychologia* **2017**, *106*, 31–41. [[CrossRef](#)] [[PubMed](#)]
33. Scholkmann, F.; Tachtsidis, I.; Wolf, M.; Wolf, U. Systemic physiology augmented functional near-infrared spectroscopy: A powerful approach to study the embodied human brain. *Neurophotonics* **2022**, *9*, 030801. [[CrossRef](#)] [[PubMed](#)]
34. Dravida, S.; Noah, J.A.; Zhang, X.; Hirsch, J. Comparison of oxyhemoglobin and deoxyhemoglobin signal reliability with and without global mean removal for digit manipulation motor tasks. *Neurophotonics* **2018**, *5*, 011006. [[CrossRef](#)]
35. Pereira, J.; Direito, B.; Luhrs, M.; Castelo-Branco, M.; Sousa, T. Multimodal assessment of the spatial correspondence between fNIRS and fMRI hemodynamic responses in motor tasks. *Sci. Rep.* **2023**, *13*, 2244. [[CrossRef](#)]
36. Sassaroli, A.; Frederick, B.B.; Tong, Y.; Renshaw, P.; Fantini, S. Spatially weighted BOLD signal for comparison of functional magnetic resonance imaging and near-infrared imaging of the brain. *Neuroimage* **2006**, *33*, 505–514. [[CrossRef](#)]
37. Cui, X.; Bray, S.; Bryant, D.M.; Glover, G.H.; Reiss, A.L. A quantitative comparison of NIRS and fMRI across multiple cognitive tasks. *Neuroimage* **2011**, *54*, 2808–2821. [[CrossRef](#)]
38. Strangman, G.; Culver, J.P.; Thompson, J.H.; Boas, D.A. A quantitative comparison of simultaneous BOLD fMRI and NIRS recordings during functional brain activation. *Neuroimage* **2002**, *17*, 719–731. [[CrossRef](#)] [[PubMed](#)]
39. Hocke, L. Automatic Motion-based artifact reduction algorithm for fNIRS in concurrent functional Magnetic Resonance Imaging studies (AMARA-fMRI). In Proceedings of the NIR 2019, Gold Coast, Australia, 17 September 2019.

Disclaimer/Publisher’s Note: The statements, opinions and data contained in all publications are solely those of the individual author(s) and contributor(s) and not of MDPI and/or the editor(s). MDPI and/or the editor(s) disclaim responsibility for any injury to people or property resulting from any ideas, methods, instructions or products referred to in the content.